The influence of the graphite mechanical properties on the constitutive response of a ferritic ductile cast iron – A micromechanical FE analysis

Andriollo, Tito; Thorborg, Jesper; Hattel, Jesper Henri

Published in:
Proceedings of the XIII International Conference on Computational Plasticity

Publication date:
2015

Document Version
Publisher's PDF, also known as Version of record

XIII International Conference on Computational Plasticity. Fundamentals and Applications
COMPLAS XIII
E. Oñate, D.R.J. Owen, D. Peric and M. Chiumenti (Eds)

THE INFLUENCE OF THE GRAPHITE MECHANICAL PROPERTIES ON THE CONSTITUTIVE RESPONSE OF A FERRITIC DUCTILE CAST IRON – A MICROMECHANICAL FE ANALYSIS

TITO ANDRIOLLO[*], JESPER THORBORG[*†] AND JESPER HATTEL[*]

[*] Department of Mechanical Engineering, Technical University of Denmark (DTU)
Produktionstorvet, Building 425, 2800 Kgs. Lyngby, Denmark
e-mail: titoan@mek.dtu.dk

[†] MAGMA GmbH, D-52072 Aachen, Germany

Key words: Computational Plasticity, Damage, Ductile Cast Iron, Micro-mechanics.

Abstract. In the present paper a micro-mechanical approach is used to investigate the influence of the graphite mechanical properties on the loading response in the early deformation range of ductile cast iron. A periodic unit cell composed by a single graphite nodule embedded in a uniform ferritic matrix is considered and elasto-plastic behavior of both constituents is assumed; damage evolution in the ductile matrix is taken into account via Lemaitre's isotropic model. Full 3D and 2D plane-stress finite element analyses are performed to simulate the loading conditions experienced by nodules located in the bulk as well as on the material surface. The effects of residual stresses arising during the manufacturing process are also accounted for. It is shown that the constitutive response of the equivalent composite medium can match ductile cast iron only if the graphite Young's modulus value lies within a certain interval, which differs from that reported in previous works on the subject. Experimental support for the numerical results is provided.

1 INTRODUCTION

From a metallurgical viewpoint, ductile cast iron (DCI) is a ternary Fe-C-Si alloy composed by graphite nodules embedded in a metallic matrix, which may have different microstructures according to chemical composition, cooling rate and heat treatment. In the last decades, the demand for DCI products has increased steadily, mainly due to the excellent combination of ductility, strength and castability that such material can offer at a very competitive price [1].

Traditionally, at least from a mechanical perspective, DCI has almost always been assumed to behave as a porous material, where the graphite nodules are simply considered to act as voids. This assumption stems primarily from the low hardness values characterizing such graphitic morphologies [2][3] and the weak strength of the matrix-nodule interface [4], which have often motivated the application of Gurson's model [5] and its various modifications [6] for the study of the DCI constitutive response. Examples of such analyses may be found in the work of Steglich & Brocks [7] and Berdin et al. [4]. Micromechanical unit cell models based on spherical cavities embedded in a matrix of pearlite and ferrite have also been proposed [8].

Nomenclature

$\bar{\varepsilon}_{ij}$	Volume average of total strain tensor	D	Damage variable
$\bar{\sigma}_{ij}$	Volume average of the stress tensor	$S,\ s$	Lemaitre's damage evolution parameters
R_v	Triaxiality function	Y	Energy release rate
s_{ij}	Deviatoric part of the stress tensor	f	Yield function
δ_{ij}	Kronecker delta	$k,\ n$	Isotropic hardening parameters
$\varepsilon_{ij}^{tot},\ \varepsilon_{ij}^{e},\ \varepsilon_{ij}^{p}$	Total, elastic, plastic strain tensor	p	Equivalent Von Mises plastic strain
σ_{ij}	Stress tensor	p_{crit}	Critical effective plastic strain for damage evolution
σ_e	Equivalent Von Mises stress		
$\sigma_y,\ \sigma_y^0$	Actual, initial yield stress	r	Hardening variable
E	Young's modulus	α	Thermal expansion coefficient
v	Poisson's ratio	λ	Plastic multiplier

Nevertheless, there are clear indications suggesting that the voided matrix assumption is likely to be overly simplified and unable to capture some peculiar phenomena observed for DCI, as discussed in [9] and in [10]. A partial explanation for the lack of analyses taking the behavior of both microscopic constituents into account is probably the absence of valid experimental data for the material properties of the graphitic phase. One of the very few attempts to characterize the non-linear mechanical response of DCI without invoking the voided matrix assumption was made by Bonora & Ruggiero [11]. In their axisymmetric micromechanical analysis, graphite spheroids were modeled as isotropic linear elastic spheres, whose Young's modulus was determined as the value providing the closest agreement between the composite equivalent stiffness and the experimentally measured stiffness for DCI. The influence of residual stresses driven by the thermal expansion coefficient mismatch between the matrix and the nodules during manufacturing was also accounted for by these authors, and turned out to have a great impact on the overall analysis.

As recent microscopy investigations confirm [12], real graphite nodules are by all means non-homogeneous and non-isotropic. However, given the almost total absence of data concerning their mechanical properties, it still makes sense to determine their "best approximation" in terms of a simple isotropic material on the basis of the response generated at the macroscopic level.

It is hence the purpose of the present study to extend and improve Bonora & Ruggiero's findings by examining aspects initially overlooked by the former authors. Specifically, nodules located on the surface as well as in the bulk of the material are considered and a threshold is set on the maximum graphite load carrying capacity. The quality of the isotropic approximation is evaluated by comparing values of equivalent macroscopic Young's modulus and Poisson's ratio with those typical for ferritic DCI in the early deformation range.

2 MICROMECHANICAL UNIT CELL MODEL

The DCI microstructure is assumed to be constituted by spherical graphite particles of equal size regularly dispersed in a homogeneous ferritic matrix. The bulk material is therefore schematized as a periodic cubic unit cell with a single central spherical nodule, as shown in figure 1. The ratio between nodule diameter and cell side is set to 0.61, in order to achieve a volumetric graphite concentration of 12 %. This is approximately the value found in GJS 400-15 DCI, which will be taken as reference material throughout the analysis.

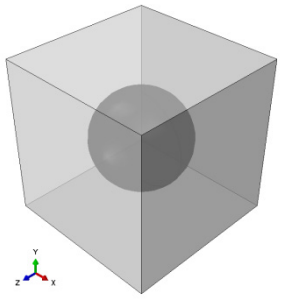

Figure 1: Micromechanical periodic unit cell representing the microstructure of DCI.

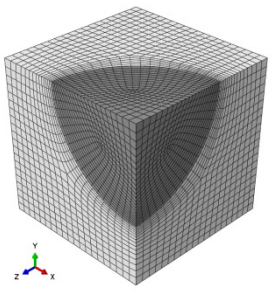

Figure 2: Geometry and mesh used in the numerical simulations.

Due to geometrical considerations, only 1/8 of the unit cell is analyzed, as figure 2 shows. Symmetry boundary conditions are applied on the three faces of the cube intersecting the graphite nodule, whereas periodic boundary conditions are imposed on the other faces according to the procedure described in [13], in order to fulfill continuity of displacements and surface tractions with the surrounding microstructure. Similarly to Bonora & Ruggiero, the boundary between the nodule and the matrix is modeled as a frictionless contact interface, with no tensile strength in the normal direction, as a consequence of the weak bonding between ferrite and graphite.

The mesoscopic initial Young's modulus E_{DCI} and Poisson's ratio ν_{DCI} for the periodic unit cell upon loading are defined as:

$$E_{DCI} = \lim_{\bar{\varepsilon}_{11}\to 0}\left(\frac{\partial\bar{\sigma}_{11}}{\partial\bar{\varepsilon}_{11}}\right), \qquad \nu_{DCI} = -\frac{\bar{\varepsilon}_{22}}{\bar{\varepsilon}_{11}} \tag{1}$$

where $\bar{\sigma}_{11}$, $\bar{\varepsilon}_{11}$ and $\bar{\varepsilon}_{22}$ denote normal components of the mesoscopic stress and strain tensor, given by the average over the unit cell volume of the corresponding microscopic quantities:

$$\bar{\sigma}_{11} = \frac{1}{V}\int_V \sigma_{11}dV\,, \quad \bar{\varepsilon}_{11} = \frac{1}{V}\int_V \varepsilon_{11}dV\,, \quad \bar{\varepsilon}_{22} = \frac{1}{V}\int_V \varepsilon_{22}dV \tag{2}$$

In addition to the 3D cell just described, a similar 2D square periodic unit cell with a circular central nodule subjected to plane-stress conditions has also been developed. It is supposed to be representative of the material behavior close to the stress-free surface of a generic DCI component. Further details may be found in [10].

3 CONSTITUENTS MATERIAL BEHAVIOR

3.1 Mechanical behavior of the ferritic matrix

Ferrite in DCI is a soft metallic phase characterized by high ductility and moderate yield strength, especially in the vicinity of nodules due to migration of carbon atoms to the graphitic phase. Therefore, it seems appropriate to describe its constitutive response on the basis of Lemaitre's isotropic damage model [14] with isotropic hardening, whose equations in Cartesian components are summarized as follows:

- additive strain decomposition:

$$\varepsilon_{ij}^{tot} = \varepsilon_{ij}^{e} + \varepsilon_{ij}^{p} + \delta_{ij}\alpha\Delta T \tag{3}$$

- elastic constitutive law:

$$\frac{\sigma_{ij}}{1-D} = \frac{E}{1+\nu}\left[\varepsilon_{ij}^{e} + \frac{\nu}{1-2\nu}\delta_{ij}\varepsilon_{kk}^{e}\right] \tag{4}$$

- flow rule:

$$\dot{\varepsilon}_{ij}^{p} = \frac{3s_{ij}}{2\sigma_e}\frac{\dot{\lambda}}{1-D} \tag{5}$$

- yield function:

$$f = \frac{\sigma_e}{1-D} - \sigma_y(r) \leq 0, \qquad \sigma_e = \left(\frac{3}{2}s_{ij}s_{ij}\right)^{1/2} \tag{6}$$

- isotropic hardening rule:

$$\sigma_y = k(r+r_0)^n, \qquad r_0 = \left(\frac{\sigma_y^0}{k}\right)^{1/n} \tag{7}$$

- effective plastic strain increment and hardening parameter increment:

$$\dot{p} = \frac{\dot{r}}{1-D}, \qquad \dot{r} = \dot{\lambda} \tag{8}$$

- damage evolution law:

$$\dot{D} = \left(\frac{Y}{S}\right)^{s}\dot{p}, \qquad if\ p > p_{crit} \tag{9}$$

- energy release rate:

$$Y = \frac{\sigma_e^2 R_v}{2E(1-D)^2}, \qquad R_v = \frac{2}{3}(1+\nu) + 3(1-2\nu)\left(\frac{\sigma_{kk}}{3\sigma_e}\right)^2 \tag{10}$$

- consistency condition:

$$f \leq 0, \qquad \dot{\lambda} \geq 0, \qquad f\dot{\lambda} = 0 \tag{11}$$

It may be noticed that 9 material parameters are required: 3 thermo-elastic (E, ν, α), 3 related to plastic flow (σ_y^0, k, n) and finally 3 related to damage (p_{crit}, S, s). In principle, an additional parameter specifying the conditions at which crack nucleation occurs would be necessary: however, in the present analyses damage never exceeds 0.1, which is well below the critical fracture initiation threshold for common metals and alloys.

In table 1 values for Young's modulus, thermal expansion coefficient and initial yield stress are reported over a wide range of temperatures; Poisson's ratio is assumed to have a constant value of 0.3 [15]. The remaining five parameters have been determined on the basis of the experimental stress-strain curve at room temperature for ferrite reported in [15] as follows:

- an analytical solution to equations (3)-(11) for uniaxial tensile loading has been calculated;
- by means of an inverse analysis performed using MATLAB, the best set of parameters has been selected according to a least square fitting of the experimental data.

A detailed discussion of the abovementioned procedure is reported in [16]; calculated values are given in table 2. As no information is available for the post-yielding behavior of the ferritic matrix at higher temperatures, plastic flow and damage evolution parameters are assumed to be constant, except for the temperature dependence of the initial yield stress previously mentioned. Time-dependent deformation mechanisms are also neglected.

Table 1: Material properties for ferritic matrix (after Bonora & Ruggiero [11]).

Temperature (°C)	Young's modulus (GPa)	Thermal exp. coefficient ($x10^{-5}$ °C^{-1})	Initial yield stress (MPa)
25	210.0	1.25	297
250	153.8	1.50	194
500	102.5	1.60	137
750	41.4	-	96
900	20.0	-	70
1000	0.1	2.40	60

Table 2: Plastic flow and damage evolution parameters for ferritic matrix.

Plastic flow factor *k* (MPa)	Plastic flow exponent *n*	Damage factor *S* (MPa)	Damage exponent *s*	Critical eff. plastic strain p_{crit} (mm/mm)
818.0	0.245	0.357	0.167	$5.33x10^{-3}$

3.2 Mechanical behavior of the graphite nodules

As already stated in the introduction, the purpose of the present study is to determine the best possible approximation of the graphite nodules achievable using a homogeneous isotropic material model. In order to keep the number of unknown parameters at a reasonable level, a simple time-independent linear elastic-perfectly plastic material behavior is assumed, based on the J2-flow theory of plasticity. Similarly to Bonora & Ruggiero, Poisson's ratio and thermal expansion coefficient are set to be the same as for bulky reactor graphite, namely ν_g = 0.15 and $\alpha_g = 2.5x10^{-6}$ °C^{-1} respectively; the other two missing parameters, Young's modulus and yield stress, are varied systematically to obtain different equivalent constitutive responses of the unit cell. It is worth remarking that no temperature dependence of any of the material properties is considered.

4 NUMERICAL ANALYSIS SETUP

Finite element analyses of the micromechanical unit cell are performed using the commercial software ABAQUS. The mesh adopted is shown in figure 2 and it is constituted by approximately 15000 hexahedral 2nd order elements with reduced integration. A small-strain formulation in combination with a non-linear numerical solution procedure based on the full Newton-Raphson scheme is chosen, and the contact condition at the matrix-nodule interface is enforced via the augmented-Lagrange method. Integration of the Lemaitre's damage equations at the local level in the ferritic matrix is accomplished by a user-defined material subroutine, according to the implicit scheme proposed in [17], where a suitable expression for the consistent tangent modulus is also suggested.

Each numerical analysis is run by initially applying a uniform temperature decreased from T_i = 1000 °C down to room temperature to the entire unit cell, with the aim of simulating the cooling process occurring during manufacturing of a generic DCI component. The specific choice of T_i is made primarily to make the results comparable with Bonora & Ruggiero's findings; it is the authors' belief, however, that a lower temperature, below the eutectoid transformation, should be more appropriate.

After cooling, an equivalent mesoscopic strain $\bar{\varepsilon}_{11}$ of $5x10^{-3}$ is progressively imposed to

investigate the unit cell behavior during "uniaxial" tension. This is achieved in 50 increments by displacing the unit cell face pointing in the negative x-direction by the amount needed.

A first set of simulations is performed by varying the graphite Young's modulus in the range 0.1 to 500 GPa, while keeping its yield strength very high, which is equivalent to assuming linear elastic behavior of the nodules. After that, the procedure is repeated setting the graphite yield strength $\sigma_{y,g}$ in sequence to 100, 50 and 25 GPa, which span the range of tensile strengths recorded for reactor graphite [18].

5 RESULTS

5.1 Linear elastic graphite

The influence of the nodule stiffness on the macroscopic Young's modulus calculated according to equation (1) is shown in figure 3, where curves corresponding to the 3D and 2D plane-stress unit cell formulations are compared with the axisymmetric model of Bonora & Ruggiero. It is worth mentioning that reference values for GJS 400-15 DCI are assumed here to lie in the interval 167-170 GPa [19], which is deemed more appropriate than the range 148-155 GPa considered by the former authors for this type of alloy.

Focusing on the curve corresponding to the 3D formulation, 3 different stages can be identified as the graphite Young's modulus is gradually increased: a very first one in which E_{DCI} exhibits a small growth with E_g, a second one in which E_{DCI} drops abruptly to approximately 60 % of its initial value, and finally a third one in which E_{DCI} returns to increase monotonically. As pointed out in [10], this particular behavior is related to the twofold effect played by an increase in the graphite stiffness: from one side, it makes the entire unit cell stiffer, as the nodule offers greater resistance to being deformed to a horizontal "oval" shape by the surrounding matrix during tensile loading; from the other side, it drives higher residual stresses at the end of the cooling stage, increasing the risk of promoting plastic deformation in the matrix, with consequent loss of stiffness.

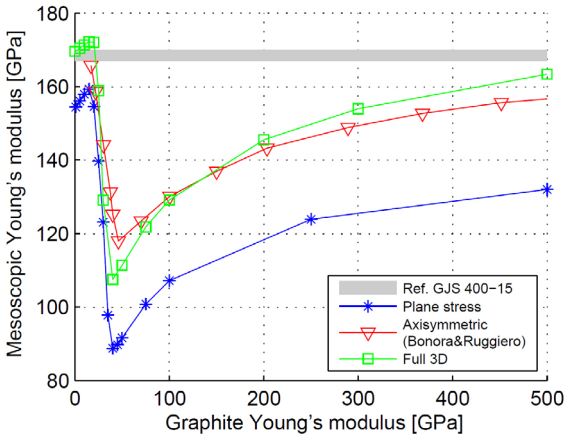

Figure 3: Predicted equivalent macroscopic Young's modulus as a function of the graphite stiffness, for different unit cell geometries. Linear elastic graphite behavior is assumed.

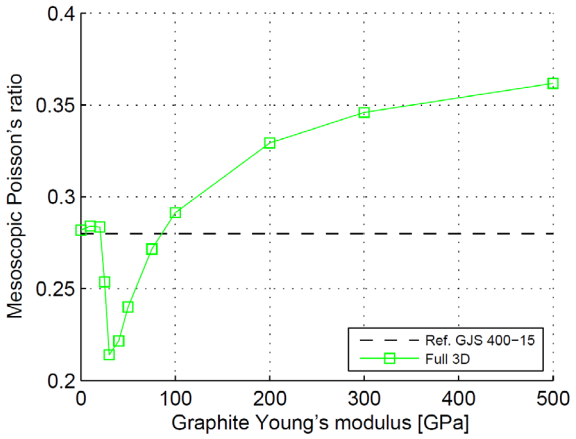

Figure 4: Predicted equivalent macroscopic Poisson's ratio as a function of the graphite stiffness, for the 3D unit cell geometry. Linear elastic graphite behavior is assumed.

The reason behind this 3-stage behavior can be better understood by looking at figure 5. As long as $E_g < 20$ GPa, the entire unit cell behaves elastically under initial loading. However, as E_g is increased further, the higher residual stresses arising from the thermal expansion coefficient mismatch between ferrite and graphite become sufficient to promote plastic yielding and damage evolution in the matrix, causing the dramatic macroscopic stiffness drop visible in the second stage. Once plasticity has spread through the entire cell cross-section, further matrix yielding produces a much less detrimental effect on E_{DCI}, which starts growing again due to the increase in the nodule elastic stiffness.

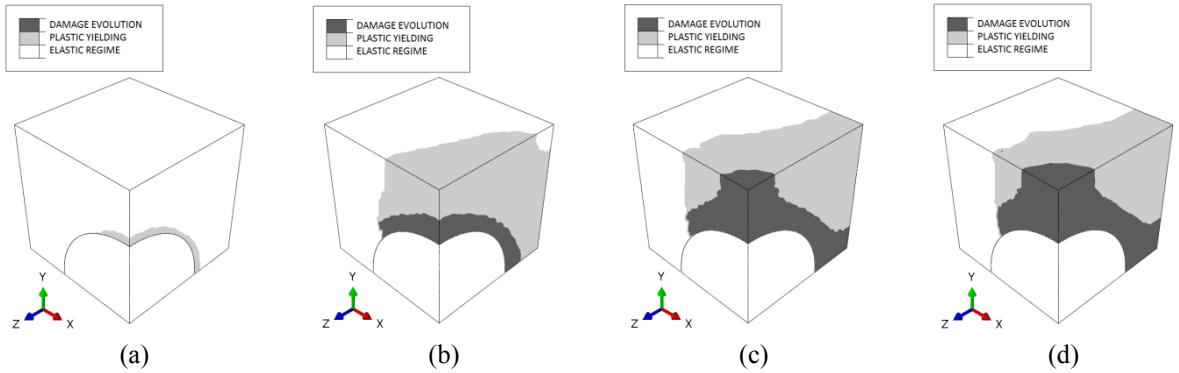

Figure 5: Plastic yielding and damage evolution in the ferritic matrix after the first load increment, for selected values of graphite Young's modulus E_g: (a) 20 GPa, (b) 30 GPa, (c) 40 GPa and (d) 50 GPa. Linear elastic graphite behavior is assumed.

With focus again on figure 3, it is clear that the axisymmetric formulation is in very good agreement with the 3D model, except for the absence of the initial elastic stage at low E_g values, which is neglected in Bonora & Ruggiero's analysis. The 2D plane-stress formulation provides results similar to those obtained for the full 3D case, the only difference being the vertical shift of the corresponding curves. This is probably due to the fact that a graphite 3D volume fraction of 12 % does not correspond, mechanically speaking, to a graphite 2D area fraction of the same value (which was the criterion used for setting up the 2D plane-stress unit cell).

Turning now the attention to figure 4, it may be recognized that the predicted macroscopic Poisson's ratio shows the same kind of 3-stage behavior discussed in the previous paragraphs. As figure 5 shows, plasticity initially develops mainly perpendicularly to the loading direction, giving little contribution to the lateral unit cell contraction: this is why ν_{DCI} exhibits a marked decrease in the range $E_g \approx 20$-40 GPa. At higher E_g values, plastic incompressibility takes over, and ν_{DCI} increases monotonically well beyond the reference value for GJS 400-15 DCI.

5.2 Elastic-perfectly plastic graphite

The effects of finite graphite yield strength values on the predicted macroscopic "elastic" constants of the 3D micromechanical unit cell are shown in figure 6 and figure 7. It appears that significant deviations in the results are visible only when the graphite Young's modulus is above 100 GPa; below that threshold, the curves are almost indistinguishable. The reason is that during the cooling stage the stress field developing in the nodule is mainly hydrostatic.

Therefore, no yielding can occur according to the J2-flow theory of plasticity. During subsequent loading, deviatoric stress components build up, but they are not sufficient to cause appreciable amount of yielding/damage, at least within the small deformation range investigated. This finds confirmation in figure 8, which shows that the graphite yield stress has a negligible influence on the overall macroscopic stress-strain curves.

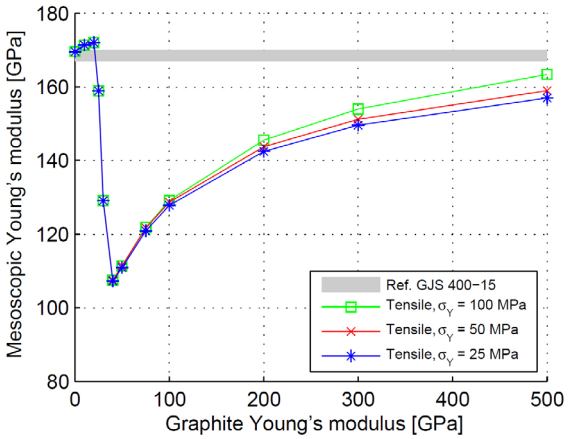

Figure 6: Predicted macroscopic Young's modulus for the 3D unit cell as a function of the graphite stiffness, for 3 different values of the graphite yield strength.

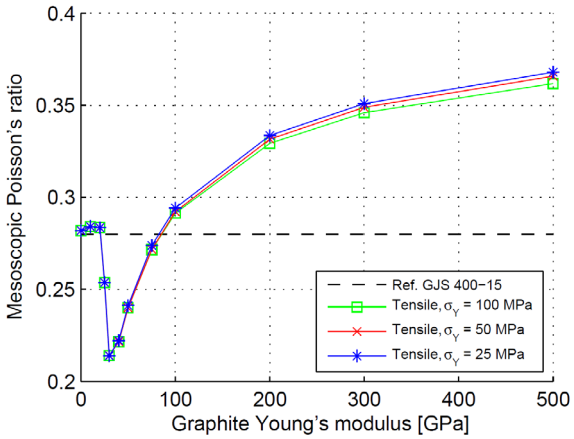

Figure 7: Predicted macroscopic Poisson's ratio for the 3D unit cell as a function of the graphite stiffness, for 3 different values of the graphite yield strength.

The situation is completely different for the 2D plane-stress formulation, where shrinkage of the matrix during cooling creates stresses in the nodule with both hydrostatic and deviatoric components. As a consequence, when the graphite yield stress is gradually decreased, plastic flow occurs in the nodule: this relieves the stress field in the matrix, which at a certain point simply remains in the elastic regime, even upon initial loading. The transition is captured in figure 9, where for sufficiently low values of the graphite yield stress, the 3-stage behavior is replaced by a single stage with monotonic growth of E_{DCI} with E_g.

It should be kept in mind, however, that the choice of adopting the J2-flow formulation for the graphite has been dictated by the necessity of setting, in the simplest way, a maximum load carrying capacity for the nodules. There are no solid grounds to sustain that such theory really reflects the physical behavior of the graphite nodules. This means that other plasticity formulations, perhaps including the hydrostatic term, might be more suitable. In addition, only residual stresses arising from differences in the thermal expansion coefficient have been considered. To make the analysis more realistic, other sources of stresses, like non-uniform cooling conditions, mechanical constraints, etc. should be included, which might lead to the occurrence of deviatoric stresses in the nodules as well. Therefore, the results shown in figure 6 and figure 7 should be taken with care.

6 CONCLUSIONS

In the present study the possibility of considering graphite nodules in a ferritic DCI as homogenous and isotropic from a micromechanical viewpoint has been investigated. The analysis extends previous works on the subject along three main directions: the behavior of

bulk and surface material is considered, a threshold is set on the maximum nodule load carrying capacity and the predicted properties of the equivalent macroscopic medium are compared to the real DCI material in terms of both initial Young's modulus and Poisson's ratio.

Assuming the graphite Poisson's ratio to be fixed at 0.15, an increase of the nodule stiffness beyond the critical threshold promoting yielding in the matrix at the beginning of loading leads to: A) a too low equivalent stiffness and B) a too large variation of the equivalent Poisson's ratio compared to the reference values for GJS 400-15 DCI. Therefore, it seems appropriate to conclude that if an isotropic approximation is sought, the graphite Young's modulus has to lie below the critical threshold for yielding, i.e. below approximately 20 GPa.

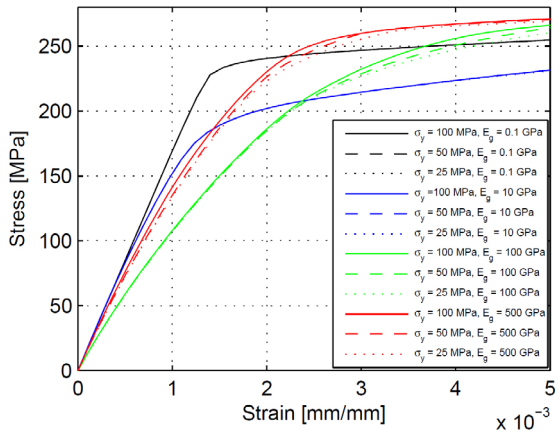

Figure 8: Macroscopic stress-strain curves up to 0.5% deformation, for graphite Young's modulus values of 0.1, 10, 100, 500 GPa and yield strength values of 25, 50, 100 MPa.

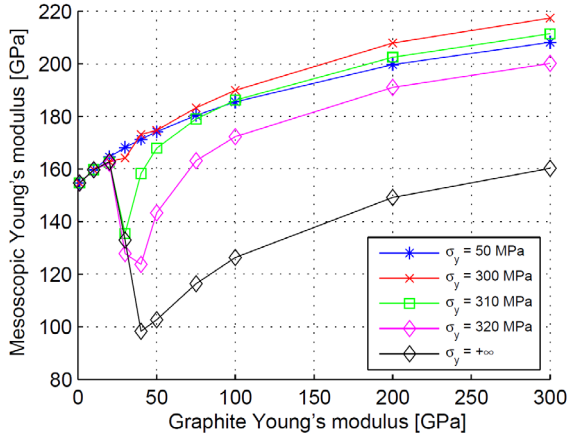

Figure 9: Predicted macroscopic Young's modulus for the 2D plane-stress unit cell as a function of the graphite stiffness, for selected values of the graphite yield strength.

REFERENCES

[1] C. Labrecque and M. Gagne, Review ductile iron: 50 years of continuous development, *Can. Metall. Q.* (1998) **37**: 343–378.

[2] S.K. Pradhan, B.B. Nayak, S.S. Sahay and B.K. Mishra, Mechanical properties of graphite flakes and spherulites measured by nanoindentation, *Carbon N. Y.* (2009) **47**: 2290–2292.

[3] P. Dierickx, C. Verdu, A. Reynaud and R. Fougeres, A study of physico-chemical mechanisms responsible for damage of heat treated and as-cast ferritic spheroïdal graphite cast irons, *Scr. Mater.* (1996) **34**: 261–268.

[4] C. Berdin, M.J. Dong and C. Prioul, Local approach of damage and fracture toughness for nodular cast iron, *Eng. Fract. Mech.* (2001) **68**: 1107–1117.

[5] A. Gurson, Continuum theory of ductile rupture by void nucleation and growth: Part 1 - Yield criteria and flow rules for porous ductile media, *J. Eng. Mater. Technol. ASME.* (1977) **99**: 2 – 15.

[6] V. Tvergaard, Analysis of the cup-cone fracture in a round tensile bar, *ACTA Metall.* (1984) **32**: 157 – 169.
[7] D. Steglich and W. Brocks, Micromechanical modeling of damage and fracture of ductile materials, *Fatigue Fract. Eng. Mater. Struct.* (1998) **21**: 1175–1188.
[8] G. Nicoletto, L. Collini, R. Konečná and E. Riva, Analysis of Nodular Cast Iron Microstructures for Micromechanical Model Development, *Strain*. (2006) **42**: 89–96.
[9] V. Di Cocco, F. Iacoviello and M. Cavallini, Damaging micromechanisms characterization of a ferritic ductile cast iron, *Eng. Fract. Mech.* (2010) **77**: 2016–2023.
[10] T. Andriollo, J. Thorborg and J. Hattel, Modeling of damage in ductile cast iron - The effect of including plasticity in the graphite nodules, in: 14th Int. Conf. Model. Cast. Weld. Adv. Solidif. Process., 2015.
[11] N. Bonora and A. Ruggiero, Micromechanical modeling of ductile cast iron incorporating damage. Part I: Ferritic ductile cast iron, *Int. J. Solids Struct.* (2005) **42**: 1401–1424.
[12] K. Theuwissen, M.-C. Lafont, L. Laffont, B. Viguier and J. Lacaze, Microstructural Characterization of Graphite Spheroids in Ductile Iron, *Trans. Indian Inst. Met.* (2012) **65**: 627–631.
[13] A. Drago and M. Pindera, Micro-macromechanical analysis of heterogeneous materials: Macroscopically homogeneous vs periodic microstructures, *Compos. Sci. Technol.* (2007) **67**: 1243–1263.
[14] J. Lemaitre, A continuous damage mechanics model for ductile fracture, *J. Eng. Mater. Technol. ASME*. (1985) **107**: 83 – 89.
[15] K.S. Zhang, J.B. Bai and D. François, Ductile fracture of materials with high void volume fraction, *Int. J. Solids Struct.* (1999) **36**: 3407–3425.
[16] T. Andriollo, J. Thorborg and J. Hattel, Analytical solution to the 1D Lemaitre's isotropic damage model and plane stress projected implicit integration procedure, *Appl. Math. Model.* (2015) , submitted.
[17] E. de Souza Neto, A fast, one-equation integration algorithm for the Lemaitre ductile damage model, *Commun. Numer. Methods Eng.* (2002) **18**: 541–554.
[18] R. Taylor, R.G. Brown, K. Gilchrist, E. Hall, A.T. Hodds, B.T. Kelly, et al., Mechanical properties of reactor graphite, *Carbon N. Y.* (1967) **5**: 519 – 531.
[19] American Foundrymen's Society, Ductile iron handbook, 1992.